Supporting Information: Finite-temperature, Anharmonicity, and Duschinsky Effects on the Two-dimensional Electronic Spectra from Ab Initio Thermo-field Gaussian Wavepacket Dynamics

Tomislav Begušić* and Jiří Vaníček*

Laboratory of Theoretical Physical Chemistry, Institut des Sciences et Ingénierie Chimiques, Ecole Polytechnique Fédérale de Lausanne (EPFL), CH-1015, Lausanne, Switzerland

E-mail: tomislav.begusic@epfl.ch; jiri.vanicek@epfl.ch

1 Rephasing and nonrephasing signals for a three-level system within the Born-Oppenheimer approximation

Since the Eqs. (6)–(8) of the main text are rarely found in that form, let us summarize how they can be obtained from the expressions that are easily found in the literature. The third-order response function[S1,S2]

$$R^{(3)}(t_3,t_2,t_1)=\sum_{\alpha=1}^{4}[R_\alpha(t_3,t_2,t_1)-R_\alpha(t_3,t_2,t_1)^*] \tag{1}$$

can be expressed in terms of correlation functions

$$R_1(t_3,t_2,t_1)=C(t_2,t_3,t_1+t_2+t_3), \tag{2}$$

$$R_2(t_3,t_2,t_1)=C(t_1+t_2,t_3,t_2+t_3), \tag{3}$$

$$R_3(t_3,t_2,t_1)=C(t_1,t_2+t_3,t_3), \tag{4}$$

$$R_4(t_3,t_2,t_1)=C(-t_3,-t_2,t_1), \tag{5}$$

where

$$C(\tau_a,\tau_b,\tau_c)=\mathrm{Tr}[\hat{\boldsymbol{\rho}}\hat{\boldsymbol{\mu}}e^{i\hat{\mathbf{H}}\tau_a/\hbar}\hat{\boldsymbol{\mu}}e^{i\hat{\mathbf{H}}\tau_b/\hbar}\hat{\boldsymbol{\mu}}e^{-i\hat{\mathbf{H}}\tau_c/\hbar}\hat{\boldsymbol{\mu}}e^{-i\hat{\mathbf{H}}(\tau_a+\tau_b-\tau_c)/\hbar}]. \tag{6}$$

In Eq. (6), we use the bold font to denote $S\times S$ matrices representing operators acting on the electronic subspace and hat $\hat{}$ to denote operators acting on the nuclear subspace; the trace is taken over both nuclear and electronic degrees of freedom. Hence, $\hat{\boldsymbol{\rho}}=\exp(-\beta\hat{\mathbf{H}})/\mathrm{Tr}[\exp(-\beta\hat{\mathbf{H}})]$ is the full molecular density matrix, $\hat{\mathbf{H}}$ is the molecular Hamiltonian, and $\hat{\boldsymbol{\mu}}$ is the dipole moment matrix. Equations (2)–(6) can be easily compared to those found in the literature, for example, with Eqs. (3.5a)–(3.6) of Ref. S2.

We now consider only three electronic states and invoke the following approximations:

1. Born-Oppenheimer approximation: $\hat{\mathbf{H}} = \mathrm{diag}(\hat{H}_1, \hat{H}_2, \hat{H}_3)$.

2. Resonance condition: Only transitions between states 1 and 2 or 2 and 3 are allowed:

$$\hat{\boldsymbol{\mu}} = \begin{pmatrix} 0 & \hat{\mu}_{21} & 0 \\ \hat{\mu}_{12} & 0 & \hat{\mu}_{23} \\ 0 & \hat{\mu}_{32} & 0 \end{pmatrix}. \tag{7}$$

3. The system is initially in the ground electronic state, i.e., the temperature effects on the electronic subspace are neglected: $\hat{\boldsymbol{\rho}} = \mathrm{diag}(\hat{\rho}, 0, 0)$, where $\hat{\rho} = \exp(-\beta\hat{H}_1)/\mathrm{Tr}[\exp(-\beta\hat{H}_1)]$.

Then, we take the trace over the electronic subspace in Eq. (6) to arrive at

$$C(\tau_a, \tau_b, \tau_c) \approx C_1(\tau_a, \tau_b, \tau_c) + C_3(\tau_a, \tau_b, \tau_c), \tag{8}$$

where C_1 and C_3 are defined according to Eq. (8) of the main text.

Finally, as discussed in Ref. S2, under the rotating-wave approximation, the rephasing and nonrephasing signals are given by

$$S_{\mathrm{R}}(t_3, t_2, t_1) = R_2(t_3, t_2, t_1) + R_3(t_3, t_2, t_1) - R_1(t_3, t_2, t_1)^*, \tag{9}$$

$$S_{\mathrm{NR}}(t_3, t_2, t_1) = R_1(t_3, t_2, t_1) + R_4(t_3, t_2, t_1) - R_2(t_3, t_2, t_1)^*. \tag{10}$$

Although each R_α splits into two terms of the right-hand side of Eq. (8), only one of those terms remains under the rotating-wave approximation. Therefore, Eqs. (9) and (10) lead to Eqs. (6) and (7) of the main text.

2 Conjugation rules in thermo-field dynamics

In the main text, we have introduced the fictitious Hilbert space with an orthonormal basis $\{|\tilde{k}\rangle\}$, which is related to the physical system (with the orthonormal basis $\{|k\rangle\}$) through

the conjugation rules[S3]

$$(\hat{A}\hat{B})\tilde{}= \hat{\tilde{A}}\hat{\tilde{B}}, \tag{11}$$

$$(\hat{A}|\alpha\rangle)\tilde{}= \hat{\tilde{A}}|\tilde{\alpha}\rangle, \tag{12}$$

$$(a\hat{A}+b\hat{B})\tilde{}= a^*\hat{\tilde{A}}+b^*\hat{\tilde{B}}, \tag{13}$$

$$(a|\alpha\rangle+b|\beta\rangle)\tilde{}= a^*|\tilde{\alpha}\rangle+b^*|\tilde{\beta}\rangle, \tag{14}$$

where the operators ($\hat{A}$, $\hat{B}$) act on and states ($|\alpha\rangle$, $|\beta\rangle$) belong to the original (without tilde) or fictitious (with tilde) Hilbert spaces; a and b are complex numbers.

Let $|\alpha\rangle = \sum_k a_k|k\rangle$. Then, $|\tilde{\alpha}\rangle = \sum_k a_k^*|\tilde{k}\rangle$,

$$\langle\tilde{\alpha}|\tilde{\beta}\rangle = \sum_k a_k b_k^* = \langle\beta|\alpha\rangle, \tag{15}$$

and

$$\langle\tilde{\alpha}'|\hat{\tilde{A}}|\tilde{\alpha}\rangle = \langle\tilde{\alpha}'|\hat{\tilde{A}}\tilde{\alpha}\rangle = \langle\hat{A}\alpha|\alpha'\rangle = \langle\alpha|\hat{A}^\dagger|\alpha'\rangle, \tag{16}$$

where in the second step of Eq. (16) we used Eqs. (12) and (15).

We now complete the proof of the main text, namely the step connecting Eqs. (17) and (18) of the main text, as follows:

$$\langle\tilde{k}_1|e^{-i\hat{\tilde{H}}_1(\tau_a+\tau_b-\tau_c)/\hbar}|\tilde{k}_2\rangle = \langle\tilde{k}_1|\left[e^{i\hat{H}_1(\tau_a+\tau_b-\tau_c)/\hbar}\right]\tilde{}\,|\tilde{k}_2\rangle \tag{17}$$

$$= \langle k_2|\left[e^{i\hat{H}_1(\tau_a+\tau_b-\tau_c)/\hbar}\right]^\dagger|k_1\rangle \tag{18}$$

$$= \langle k_2|e^{-i\hat{H}_1(\tau_a+\tau_b-\tau_c)/\hbar}|k_1\rangle, \tag{19}$$

where in (17) we used the conjugation rules (11) and (13), in going from (17) to (18) we used Eq. (16), and in the last step we used the fact that the Hamiltonian is Hermitian.

3 Thermo-field dynamics expression for $C(\tau_a, \tau_b, \tau_c)$ beyond the Born-Oppenheimer approximation

In the main text, we invoked the Born–Oppenheimer approximation so that the thermo-field dynamics expression could be easily combined with the thawed Gaussian wavepacket dynamics. Of course, in many systems of interest, such as excitonic or multichromophoric systems, or photochemically active molecules, the coupling between electronic states must be included in the calculations. Here, we present the result beyond the Born-Oppenheimer approximation.

As in Eq. (11) of the main text, we define the thermal vacuum, now in the extended molecular (electronic and vibrational) Hilbert space:

$$|\bar{\mathbf{0}}(\beta)\rangle = \hat{\boldsymbol{\rho}}^{1/2} \sum_k |\mathbf{k}\tilde{\mathbf{k}}\rangle. \tag{20}$$

In other words, the state $|\bar{\mathbf{0}}(\beta)\rangle$ is described not only by a doubled number of vibrational coordinates, but also a doubled number of electronic degrees of freedom. Following similar steps as in the derivation of the main text, we can rewrite Eq. (6) (see Sec. 1 of the Supporting Information) as

$$C(\tau_a, \tau_b, \tau_c) = \langle \bar{\boldsymbol{\phi}}_{\tau_b,\tau_a} | \bar{\boldsymbol{\phi}}_{0,\tau_c} \rangle, \tag{21}$$

where

$$|\bar{\boldsymbol{\phi}}_{\tau,t}\rangle = e^{-i\hat{\bar{\mathbf{H}}}\tau/\hbar} \hat{\boldsymbol{\mu}} e^{-i\hat{\bar{\mathbf{H}}}t/\hbar} \hat{\boldsymbol{\mu}} |\bar{\mathbf{0}}(\beta)\rangle \tag{22}$$

and $\hat{\bar{\mathbf{H}}} = \hat{\mathbf{H}} - \hat{\tilde{\mathbf{H}}}$. The result (21) accounts for coupled electronic states and thermal population of excited electronic states. Importantly, Eq. (21) justifies the thermo-field wavepacket picture even beyond the Born–Oppenheimer approximation.

4 Rephasing and nonrephasing two-dimensional spectra

In Figs. S1 and S2, we show separately the rephasing and nonrephasing contributions to the total absorptive spectra of the main text. The rephasing spectrum exhibits a "checkerboard" pattern,[S4,S5] whereas the nonrephasing peaks appear only along the diagonal.[S6] The interesting nodal structure of the nonrephasing spectrum at $t_2 = 0$ is a consequence of the broadening. As discussed in Refs. S7 and S2, the peak lineshape exhibits a "phase twist" due to the so-called dispersive component of the broadening function. In the nonrephasing spectrum, the negative intensities about a peak centered at (Ω_1, Ω_3) appear at $(\omega_1 > \Omega_1, \omega_3 > \Omega_3)$ and $(\omega_1 < \Omega_1, \omega_3 < \Omega_3)$ [see, e.g., Fig. 3(b) of Ref. S2]. By simple addition, these negative features become enhanced in between the diagonal peaks (see Fig. S2, bottom). Contrary to general knowledge, this nodal structure does not disappear when we sum the rephasing and nonrephasing spectra (see, e.g., Fig. S3, top). Due to coherent vibrational dynamics, the nonrephasing and rephasing spectra are different. More precisely, the diagonal peaks of the nonrephasing spectrum are much stronger than the same peaks in the rephasing spectrum and, therefore, their dispersive contributions do not cancel out completely in the total spectrum.[S2,S7] Consequently, the total spectrum, given by the sum of the rephasing and nonrephasing spectra, is not necessarily composed of purely absorptive peaks. Similar pattern can be seen, for example, in Fig. 4 (leftmost panels showing spectra at $t_2 = 0$) of Ref. S8.

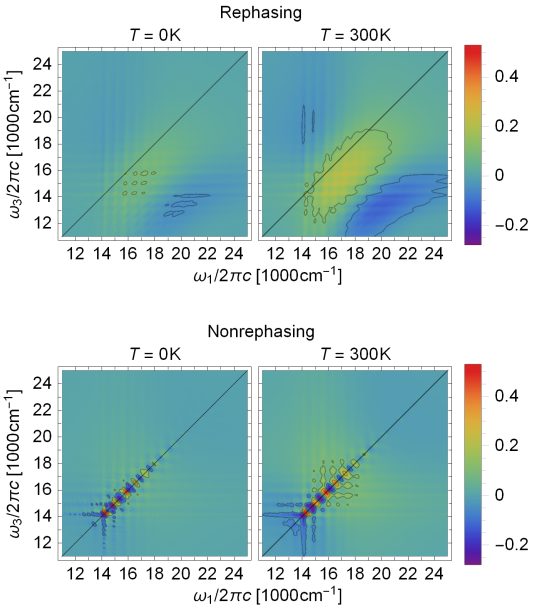

Figure S1: Rephasing (top) and nonrephasing (bottom) contributions to the two-dimensional spectra from Fig. 2 of the main text at zero temperature (left) and at $T = 300\,\mathrm{K}$ (right).

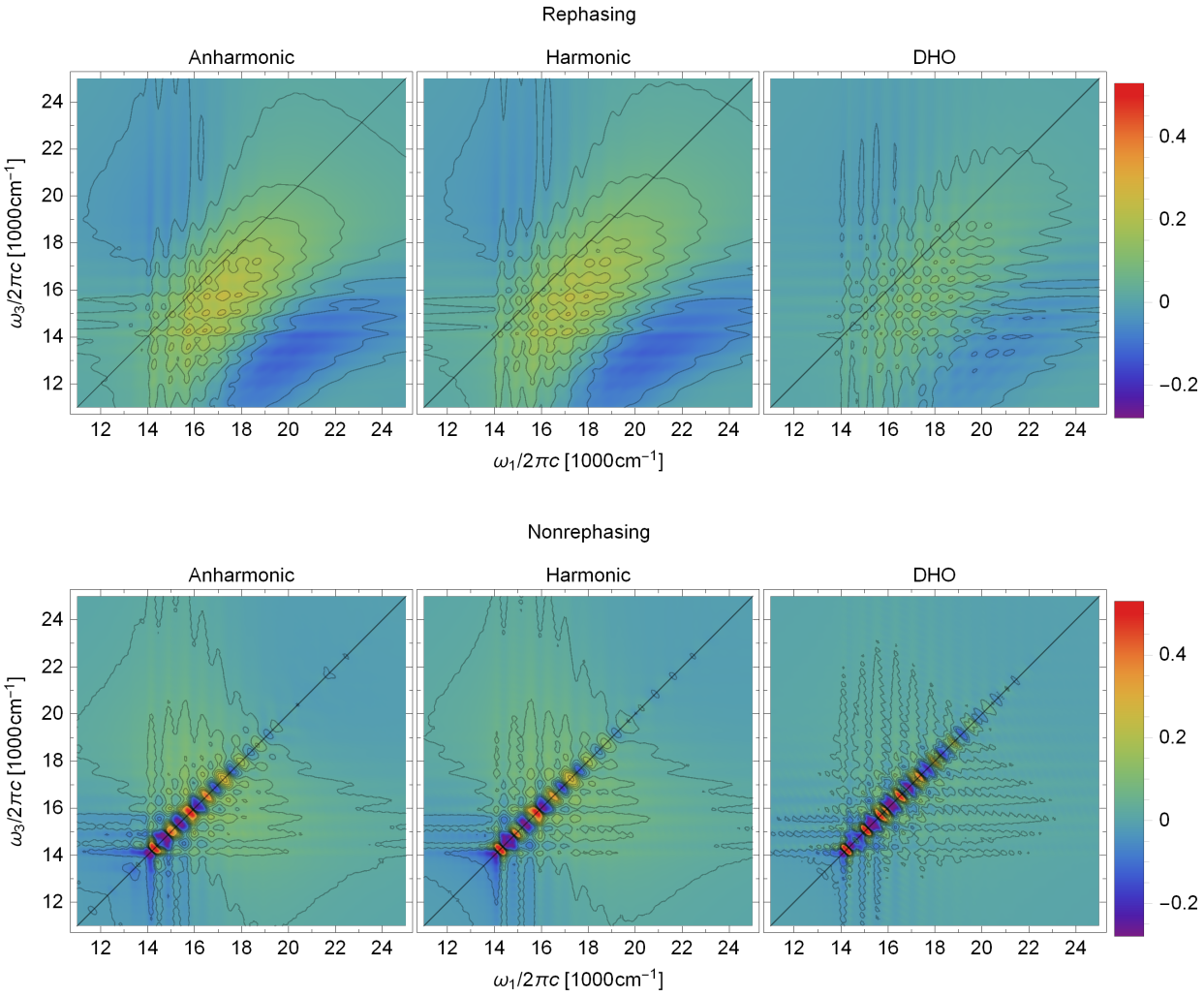

Figure S2: Rephasing (top) and nonrephasing (bottom) contributions to the two-dimensional spectra from Fig. 4 of the main text, computed with the on-the-fly ab initio single-Hessian thawed Gaussian approximation ("Anharmonic", left), harmonic approximation (middle), and the displaced harmonic oscillator (DHO) model (right).

5 Two-dimensional spectra at $t_2 > 0$

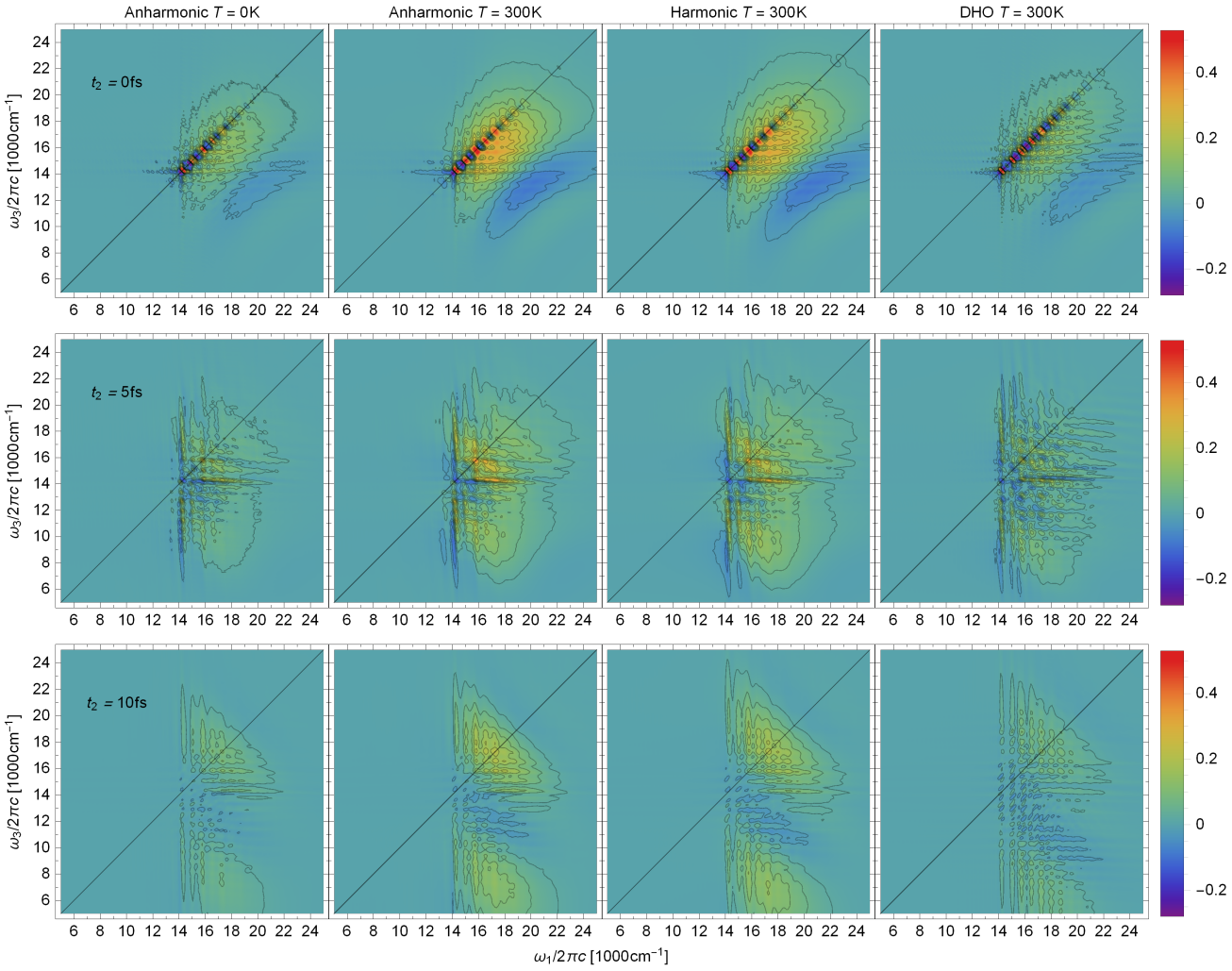

Figure S3: Two-dimensional electronic spectra [Eq. (3) of the main text] at delay times $t_2 = 0, 5, 10$ fs, computed with the on-the-fly ab initio single-Hessian thawed Gaussian approximation ("Anharmonic") at 0 K (first column) and 300 K (second column), harmonic approximation at 300 K (third column), and the displaced harmonic oscillator (DHO) at 300 K model (fourth column). Each spectrum shows the sum of the ground-state bleach and stimulated emission terms [first two terms on the right-hand sides of Eqs. (6) and (7) of the main text] corresponding to the S_1–S_0 electronic transition in azulene. At zero delay, the ground-state bleach and stimulated emission contributions are indistinguishable. However, already after 5 or 10 fs, the stimulated emission signal moves away from the diagonal, whereas the ground-state bleach spectrum remains close to the diagonal. At later t_2 delays (see Fig. S4), the stimulated emission starts returning towards the diagonal, reflecting coherent wavepacket dynamics in the excited electronic state. Indeed, the period of about 20–25 fs corresponds to the faster displaced modes (see Table S1). However, the recurrence is incomplete due to the slower dynamics in the other highly displaced modes.

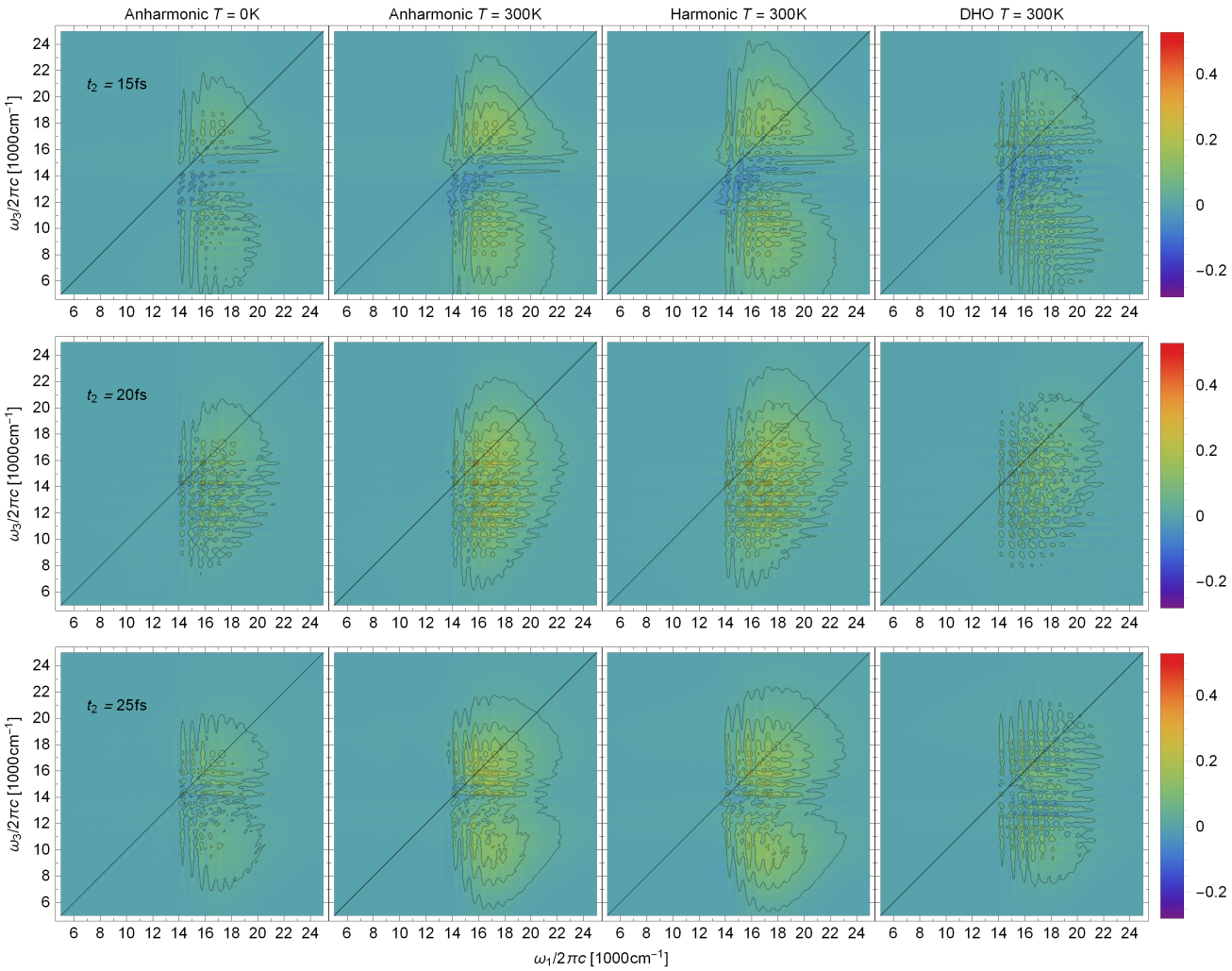

Figure S4: Same as Fig. S3 but for delay times $t_2 = 15, 20, 25$ fs.

Table S1: The most displaced modes of azulene. Ground-state frequencies ω_i of the normal modes are reported in terms of the wavenumber. The dimensionless displacements are defined as $\Delta_i = |\sqrt{\omega_i/\hbar} q_{2,i}|$, where q_2 is the excited-state minimum geometry expressed in the mass-scaled normal mode coordinates of the ground electronic state and $q_{2,i}$ is its component along mode i. Only the modes with $\Delta_i > 0.25$ are shown.

Wavenumber / cm^{-1}	Displacement
1660	0.92
1490	0.83
1425	1.22
1304	0.68
834	1.44
677	0.78
403	0.49

6 $|S_{\mathbf{R}}(t_3, 0, t_1)|$ at short t_1 and t_3 times

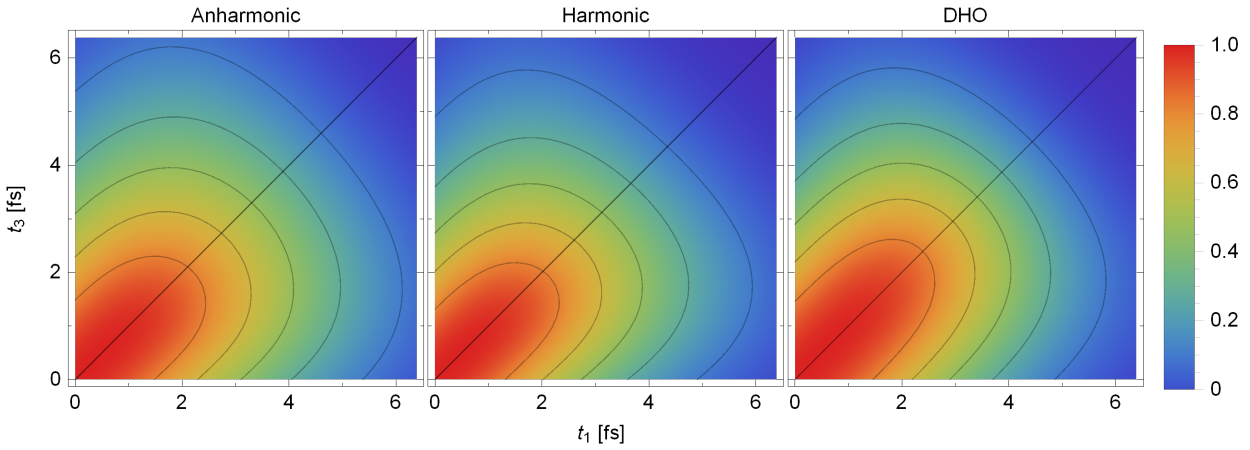

Figure S5: First 6 fs of $|S_{\mathrm{R}}(t_3, 0, t_1)|$ (see Fig. 4 of the main text) computed with the on-the-fly ab initio thawed Gaussian approximation ("Anharmonic"), harmonic approximation, and the displaced harmonic oscillator (DHO) model.

7 (A)symmetry of the rephasing and nonrephasing signals in the time domain

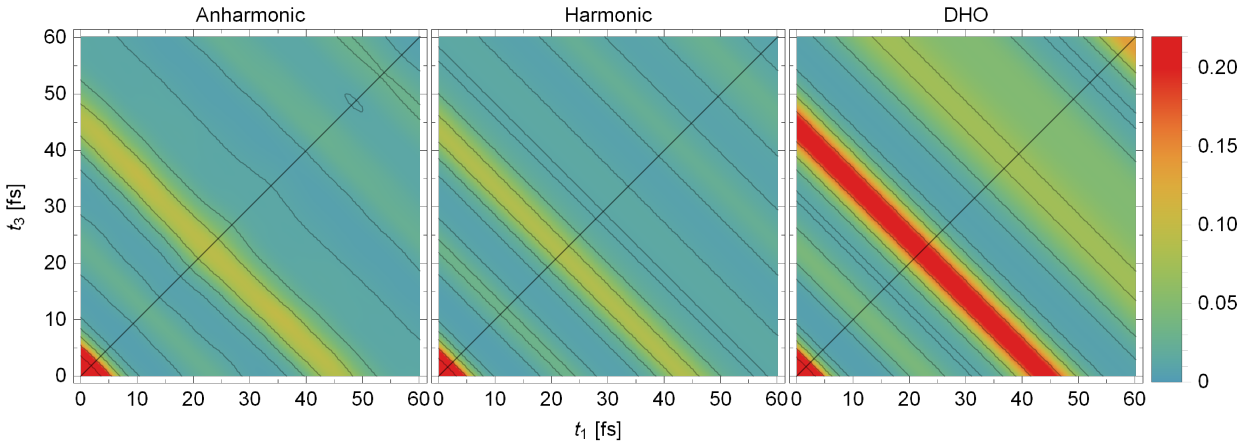

Figure S6: Absolute value of the nonrephasing time-domain signal ($|S_{\mathrm{NR}}(t_3, 0, t_1)|$) at zero time delay ($t_2 = 0$), including only the ground-state bleach and stimulated emission terms [first two terms on the right-hand side of Eq. (7) of the main text], computed with the on-the-fly ab initio single-Hessian thawed Gaussian approximation ("Anharmonic", left), harmonic approximation (middle), and the displaced harmonic oscillator (DHO) model (right) at 300 K.

In Fig. S6, we show that the absolute value of the nonrephasing signal $S_{\mathrm{NR}}(t_3, 0, t_1)$ at $t_2 = 0$ is symmetric with respect to the diagonal $t_1 = t_3$ for all three—anharmonic, harmonic, and the displaced harmonic oscillator—models, whereas the rephasing signal $|S_{\mathrm{R}}(t_3, 0, t_1)|$ (Fig. 4 of the main text) exhibits this symmetry only for the displaced harmonic oscillator model. Indeed, if we assume the Condon approximation ($\hat{\mu}_{21} \approx \mu = \text{const.}$) and include only the ground-state bleach and stimulated emission contributions, the nonrephasing signal at $t_2 = 0$ can be rewritten as a function of $t_1 + t_3$:

$$S_{\mathrm{NR}}(t_3, 0, t_1) = C_1(0, t_3, t_1 + t_3) + C_1(-t_3, 0, t_1) \tag{23}$$

$$= 2|\mu|^4 \mathrm{Tr}[\hat{\rho} e^{i\hat{H}_1(t_1+t_3)/\hbar} e^{-i\hat{H}_2(t_1+t_3)/\hbar}] \tag{24}$$

$$= S_{\mathrm{NR}}(t_1, 0, t_3) \tag{25}$$

and is, therefore, symmetric with respect to the exchange of t_1 and t_3. In going from (23) to (24), we used the definition of C_1 [Eq. (8) of the main text], the Condon approximation, the fact that $\hat{\rho}$ commutes with the ground-state vibrational Hamiltonian $\hat{H}_1$, and the cyclic property of the trace. The same, however, does not hold for the rephasing contribution:

$$S_{\mathrm{R}}(t_3,0,t_1) = 2C_1(t_1,t_3,t_3) \tag{26}$$

$$= 2|\mu|^4 \mathrm{Tr}[\hat{\rho} e^{i\hat{H}_2 t_1/\hbar} e^{i\hat{H}_1 t_3/\hbar} e^{-i\hat{H}_2 t_3/\hbar} e^{-i\hat{H}_1 t_1/\hbar}] \tag{27}$$

$$\neq 2|\mu|^4 \mathrm{Tr}[\hat{\rho} e^{i\hat{H}_2 t_3/\hbar} e^{i\hat{H}_1 t_1/\hbar} e^{-i\hat{H}_2 t_1/\hbar} e^{-i\hat{H}_1 t_3/\hbar}] \tag{28}$$

$$= S_{\mathrm{R}}(t_1,0,t_3). \tag{29}$$

Yet, within the displaced harmonic oscillator model, the symmetry is recovered for the absolute value of $S_{\mathrm{R}}(t_1,0,t_3)$. This is discussed in the following Section.

8 Symmetry of the two-dimensional signal within the second-order cumulant approximation

Within the second-order cumulant method,[S1] assuming only two electronic states (i.e., neglecting the excited-state absorption) and the Condon approximation ($\hat{\mu} \approx \mu = \text{const.}$), the components $R_\alpha(t_3,t_2,t_1)$ of the third-order response function (1) are approximated as

$$R_1(t_3,t_2,t_1) = |\mu|^4 e^{-i\omega_{21}t_1 - i\omega_{21}t_3} e^{-g(t_3)^* - g(t_1) - f_+(t_3,t_2,t_1)}, \tag{30}$$

$$R_2(t_3,t_2,t_1) = |\mu|^4 e^{i\omega_{21}t_1 - i\omega_{21}t_3} e^{-g(t_3)^* - g(t_1)^* + f_+(t_3,t_2,t_1)^*}, \tag{31}$$

$$R_3(t_3,t_2,t_1) = |\mu|^4 e^{i\omega_{21}t_1 - i\omega_{21}t_3} e^{-g(t_3) - g(t_1)^* + f_-(t_3,t_2,t_1)^*}, \tag{32}$$

$$R_4(t_3,t_2,t_1) = |\mu|^4 e^{-i\omega_{21}t_1 - i\omega_{21}t_3} e^{-g(t_3) - g(t_1) - f_-(t_3,t_2,t_1)}, \tag{33}$$

where

$$\omega_{21} = \frac{1}{\hbar}\mathrm{Tr}[(\hat{V}_2 - \hat{V}_1)\hat{\rho}] \tag{34}$$

is the thermally averaged electronic energy gap, $\hat{V}_i$ are the potential energy operators in the ground ($i = 1$) or excited ($i = 2$) electronic states,

$$g(t) = \frac{1}{\hbar^2} \int_0^t d\tau_2 \int_0^{\tau_2} d\tau_1 \mathrm{Tr}[e^{i\hat{H}_1\tau_1/\hbar} \Delta\hat{V} e^{-i\hat{H}_1\tau_1/\hbar} \Delta\hat{V}\hat{\rho}], \tag{35}$$

$\Delta\hat{V} = \hat{V}_2 - \hat{V}_1 - \hbar\omega_{21}$, and

$$f_-(t_3, t_2, t_1) = g(t_2) - g(t_2 + t_3) - g(t_1 + t_2) + g(t_1 + t_2 + t_3), \tag{36}$$

$$f_+(t_3, t_2, t_1) = g(t_2)^* - g(t_2 + t_3)^* - g(t_1 + t_2) + g(t_1 + t_2 + t_3). \tag{37}$$

For simple systems, such as a pair of harmonic potentials, exact quantum-mechanical $g(t)$ can be found analytically.[S1,S9] The second-order cumulant expansion is exact only in the special case of the displaced harmonic (Brownian) oscillator model. For general potentials, efficient classical approximations to $g(t)$ can be employed, at the price of introducing additional approximations in the evaluation of the response function (1). Remarkably, it is easy to show that, no matter how $g(t)$ is computed, the symmetry relationship

$$|R_\alpha(t_3, t_2, t_1)| = |R_\alpha(t_1, t_2, t_3)|, \qquad \alpha = 1, \ldots, 4, \tag{38}$$

holds for the four second-order cumulant expressions (30)–(33). For example, for R_3 we have

$$|R_3(t_3, t_2, t_1)|^2 = R_3(t_3, t_2, t_1)^* R_3(t_3, t_2, t_1) \tag{39}$$

$$= e^{-g(t_3)^* - g(t_1) + f_-(t_3, t_2, t_1)} e^{-g(t_3) - g(t_1)^* + f_-(t_3, t_2, t_1)^*} \tag{40}$$

$$= e^{-2\mathrm{Re}[g(t_3) + g(t_1) - f_-(t_3, t_2, t_1)]} \tag{41}$$

$$= e^{-2\mathrm{Re}[g(t_1) + g(t_3) - f_-(t_1, t_2, t_3)]} \tag{42}$$

$$= |R_3(t_1, t_2, t_3)|^2, \tag{43}$$

where (42) follows from (41) because

$$f_-(t_3,t_2,t_1) = f_-(t_1,t_2,t_3). \tag{44}$$

Similar procedure can be followed for other R_α functions, where we also need to use the relation:

$$\mathrm{Re} f_+(t_3,t_2,t_1) = \mathrm{Re} f_+(t_1,t_2,t_3). \tag{45}$$

Since the exact R_α for the displaced harmonic oscillator model can be written in the form of Eqs. (30)–(33), the proof holds in this special case as well.

Equation (38) implies that the symmetry with respect to exchanging t_1 and t_3 is present for arbitrary delay t_2. However, in experiments, one cannot measure individual components of the response function but only their linear combination. For example, the signal measured in the rephasing phase-matching direction is[S2]

$$S_\mathrm{R}(t_3,t_2,t_1) = R_2(t_3,t_2,t_1) + R_3(t_3,t_2,t_1). \tag{46}$$

Then,

$$|S_\mathrm{R}(t_3,t_2,t_1)|^2 = |R_2(t_3,t_2,t_1)|^2 + |R_3(t_3,t_2,t_1)|^2 + 2\mathrm{Re}[R_3(t_3,t_2,t_1)^* R_2(t_3,t_2,t_1)] \tag{47}$$

$$\neq |S_\mathrm{R}(t_1,t_2,t_3)|^2 \tag{48}$$

because

$$R_3(t_3,t_2,t_1)^* R_2(t_3,t_2,t_1) = e^{-g(t_3)^*-g(t_1)+f_-(t_3,t_2,t_1)} e^{-g(t_3)^*-g(t_1)^*+f_+(t_3,t_2,t_1)^*} \tag{49}$$

$$= e^{-2g(t_3)^*-2\mathrm{Re}[g(t_1)]+f_-(t_3,t_2,t_1)+f_+(t_3,t_2,t_1)^*} \tag{50}$$

$$= e^{-2g(t_3)^*-2\mathrm{Re}[g(t_1)]+2g(t_2)-2g(t_2+t_3)-2\mathrm{Re}[g(t_1+t_2)]+2\mathrm{Re}[g(t_1+t_2+t_3)]} \tag{51}$$

$$\neq e^{-2g(t_1)^*-2\mathrm{Re}[g(t_3)]+2g(t_2)-2g(t_1+t_2)-2\mathrm{Re}[g(t_2+t_3)]+2\mathrm{Re}[g(t_1+t_2+t_3)]} \tag{52}$$

$$= e^{-2g(t_1)^*-2\mathrm{Re}[g(t_3)]+f_-(t_1,t_2,t_3)+f_+(t_1,t_2,t_3)^*} \tag{53}$$

$$= R_3(t_1,t_2,t_3)^* R_2(t_1,t_2,t_3). \tag{54}$$

Nevertheless, the equality is restored at $t_2 = 0$ because $R_2(t_3,0,t_1) = R_3(t_3,0,t_1)$:

$$|S_\mathrm{R}(t_3,0,t_1)|^2 = 4|R_3(t_3,0,t_1)|^2 = 4|R_3(t_1,0,t_3)|^2 = |S_\mathrm{R}(t_1,0,t_3)|^2. \tag{55}$$

References

(S1) Mukamel, S. *Principles of nonlinear optical spectroscopy*, 1st ed.; Oxford University Press: New York, 1999.

(S2) Schlau-Cohen, G. S.; Ishizaki, A.; Fleming, G. R. Two-dimensional electronic spectroscopy and photosynthesis: Fundamentals and applications to photosynthetic light-harvesting. *Chem. Phys.* **2011**, *386*, 1–22.

(S3) Suzuki, M. Thermo Field Dynamics in Equilibrium and Non-Equilibrium Interacting Quantum Systems. *J. Phys. Soc. Jap.* **1985**, *54*, 4483–4485.

(S4) Borrego-Varillas, R.; Nenov, A.; Ganzer, L.; Oriana, A.; Manzoni, C.; Tolomelli, A.; Rivalta, I.; Mukamel, S.; Garavelli, M.; Cerullo, G. Two-dimensional UV spectroscopy: A new insight into the structure and dynamics of biomolecules. *Chem. Sci.* **2019**, *10*, 9907–9921.

(S5) Picchiotti, A.; Nenov, A.; Giussani, A.; Prokhorenko, V. I.; Miller, R. J. D.; Mukamel, S.; Garavelli, M. Pyrene, a Test Case for Deep-Ultraviolet Molecular Photophysics. *J. Phys. Chem. Lett.* **2019**, *10*, 3481–3487.

(S6) Begušić, T.; Vaníček, J. On-the-fly ab initio semiclassical evaluation of third-order response functions for two-dimensional electronic spectroscopy. *J. Chem. Phys.* **2020**, *153*, 184110.

(S7) Khalil, M.; Demirdöven, N.; Tokmakoff, A. Obtaining absorptive line shapes in two-dimensional infrared vibrational correlation spectra. *Phys. Rev. Lett.* **2003**, *90*, 4.

(S8) Anda, A.; Abramavičius, D.; Hansen, T. Two-dimensional electronic spectroscopy of anharmonic molecular potentials. *Phys. Chem. Chem. Phys.* **2018**, *20*, 1642–1652.

(S9) Zuehlsdorff, T. J.; Hong, H.; Shi, L.; Isborn, C. M. Nonlinear spectroscopy in the condensed phase: The role of Duschinsky rotations and third order cumulant contributions. *J. Chem. Phys.* **2020**, *153*, 044127.